Nuclear Medicine and Biology 144-145 (2025) 109001

Contents lists available at ScienceDirect

Nuclear Medicine and Biology

journal homepage: www.elsevier.com/locate/nucmedbio

Investigating the fate of Zirconium-89 labelled antibody in cynomolgus macaques

Takanori Sasaki [a,*,1], Sadaaki Kimura [b,1], Akihiro Noda [b], Yoshihiro Murakami [b], Sosuke Miyoshi [b], Masaru Akehi [a,e], Kazuhiko Ochiai [c], Masami Watanabe [a], Takahiro Higuchi [a,d], Eiji Matsuura [a]

[a] Faculty of Medicine, Dentistry, and Pharmaceutical Sciences, Okayama University, 2-5-1, Shikata-cho, Kita-ku, Okayama-shi, Okayama 700-8558, Japan
[b] Astellas Pharma Inc., 21 Miyukigaoka, Tsukuba-shi, Ibaraki 305-8585, Japan
[c] School of Veterinary Nursing and Technology, Faculty of Veterinary Science, Nippon Veterinary and Life Science University, 1-7-1 Kyonancho, Musashino-shi, Tokyo 180-8602, Japan
[d] Department of Nuclear Medicine and Comprehensive Heart Failure Center, University Hospital of Würzburg, Oberdürrbacher Strasse 6, 97080 Würzburg, Germany
[e] Neutron Therapy Research Center, Okayama University, 2-5-1, Shikata-cho, Kita-ku, Okayama-shi, Okayama 700-8558, Japan

ARTICLE INFO

Keywords:
PET imaging
Zirconium-89
Therapeutic antibodies
Non-human primates

ABSTRACT

Background: Preclinical pharmacokinetic studies of therapeutic antibodies in non-human primates are desired because of the difficulty in extrapolating ADME data from animal models to humans. We evaluated the pharmacokinetics of ^{89}Zr (Zirconium-89) -labelled anti-KLH human IgG and its metabolites to confirm their non-specific/physiological accumulation in healthy cynomolgus macaques. The anti-KLH antibody was used as a negative control, ensuring that the observed distribution reflected general IgG behavior rather than antigen-specific accumulation. This provides a valuable reference for comparing the biodistribution of targeted antibodies.

Methods: Selected IgG was conjugated to desferrioxamine (DFO), labelled with ^{89}Zr, and injected into healthy cynomolgus macaques. PET/CT images at the whole-body level were acquired at different time points, and standard uptake values (SUV) in regions of interest, such as the heart, liver, spleen, kidneys, bone, and muscles, were calculated. The distribution of a shortened antibody variant, ^{89}Zr-labelled Fab, as well as that of [^{89}Zr]Zr-DFO and [^{89}Zr]Zr-oxalate, the expected metabolites of ^{89}Zr- labelled IgG, was also assessed.

Results: After ^{89}Zr-labelled IgG injection, the SUV in the heart, vertebral body, and muscle decreased, in line with the ^{89}Zr concentration decrease in the circulation, whereas radioactivity increased over time in the kidneys and liver. Autoradiography of the renal sections indicated that most of the ^{89}Zr- labelled IgG radioactivity accumulated in the renal cortex. Relatively high accumulation in the kidneys was also observed in ^{89}Zr- labelled Fab-injected macaques, and renal autoradiographs of these animals showed that the renal cortex was the preferred accumulation site. However, [^{89}Zr]Zr-DFO was rapidly excreted into the urine, whereas [^{89}Zr]Zr-oxalate was highly accumulated in the epiphysis of the long bones and vertebral body.

Conclusion: In the non-human primate cynomolgus macaque, ^{89}Zr- labelled IgG accumulated in the kidneys and the liver. However, [^{89}Zr]Zr-DFO and ^{89}Zr did not accumulate in these organs. This preclinical pharmacokinetic study performed with human IgG in a non-human primate model using PET is of great significance as it sheds light on the basic fate and distribution of ^{89}Zr- labelled IgG.

1. Introduction

In recent decades, there has been much progress in antibody drug development. The indications for these products have expanded beyond their initial use in cancer and immune-inflammatory diseases, including now infections and chronic diseases such as age-related macular degeneration and hyperlipidaemia. Non-clinical safety studies of monoclonal antibodies (mAbs) performed in primates may provide

* Corresponding author.
E-mail address: t-sasaki@cc.okayama-u.ac.jp (T. Sasaki).
[1] These two authors contributed equally to this work.

https://doi.org/10.1016/j.nucmedbio.2025.109001
Received 3 November 2024; Received in revised form 2 February 2025; Accepted 13 February 2025
Available online 14 February 2025

pharmacological data comparable to those expected in humans regarding both potency and mechanism of action. Non-human primates (NHPs) are often considered the only relevant species with tissue expression patterns comparable to those of humans and immune responses that do not limit exposure. Therefore, the use of NHPs in preclinical studies on mAbs has increased [1]. Some data indicate that approximately 80 % of mAbs currently under development have potency/cross-reactivity only in NHPs and humans [2]. Furthermore, in chronic disease areas such as rheumatoid arthritis, more complex and larger studies involving NHPs may be necessary to provide greater information and safety assurance, given the variable risk/benefit ratios in some patient populations (e.g., pregnant women, children) [2].

Radiolabelling of antibody fragments has facilitated the development of therapeutic antibodies, allowing evaluation of their specificity and distribution kinetics. Various preclinical and clinical studies have revealed that radiolabelled antibodies are effective imaging probes for cancer and inflammatory diseases diagnosis [3,4]. Furthermore, radiolabelled antibodies are used in drug delivery systems such as radioimmunotherapy and theranostics. In personalised medicine, radiolabelled antibodies have acquired a central role as diagnostic and therapeutic agents; in addition, radiolabelled antibodies may be used to optimise drug development [5]. The use of radiolabelled antibodies combined with imaging techniques constitutes an effective method for the non-invasive assessment of antibody fate and distribution at the whole-body level.

Radiolabelled antibodies can be detected using single-photon emission computed tomography (SPECT) or positron emission tomography (PET). Examples of radionuclides that have been used to radiolabel antibodies and evaluated through SPECT are ^{99m}Tc, ^{123}I, ^{131}I, and ^{111}In, whereas ^{18}F, ^{68}Ga, ^{64}Cu, ^{89}Zr, and ^{124}I have been used to obtain radiolabel antibodies for PET studies. The combined use of PET and antibodies is called immuno-PET, and because of the high sensitivity and resolution power of the PET camera and the specificity of an antibody, this technology has become particularly attractive for visualizing and characterising tumours [6]. Among the various radioisotopes used for PET, the long half-life radiometal ^{89}Zr ($t_{1/2} = 78.4$ h) is one of the most suitable for immuno-PET. Due to this long half-life time, ^{89}Zr-labelled antibodies would permit long observation periods, even for several days, which may be required for the accurate pharmacodynamic analysis of substances having a long biological half-life, such as IgG. Recent advancements, such as total-body PET, further enhance the utility of ^{89}Zr-labelled antibodies by enabling whole-body imaging with higher sensitivity and efficiency, providing comprehensive insights into antibody distribution and kinetics over time [7].

The ^{89}Zr-radiolabelling procedure for antibodies commonly involves the previous attachment to the antibody of a bifunctional ligand; the desferrioxamine (DFO) derivative *p*-isothiocyanatobenzyl-DFO was developed for this purpose [8]. ^{89}Zr-production methods based on the use of small cyclotrons have been reported [9], and the usefulness of ^{89}Zr for antibody imaging in preclinical and clinical studies has been largely documented [10]. However, several questions have arisen regarding the stability of the [^{89}Zr]Zr-DFO-antibody in long-term in vivo studies, and some reports have shown increased non-specific uptake of [^{89}Zr]Zr-DFO-antibody by bones [11]. Similar findings have been reported after assessing chelated ^{89}Zr ([^{89}Zr]Zr-DFO, [^{89}Zr]Zr-oxalate) or solvated ^{89}Zr ([^{89}Zr]Zr-chloride, [^{89}Zr]Zr-phosphate) distribution in mice [12]. In this scenario, it is crucial to determine whether the ^{89}Zr metal and [^{89}Zr]Zr-DFO attachment to the antibody is stable for several days after injection to allow adequate assessment of its specificity and distribution.

To develop therapeutic antibodies, preclinical and pharmacokinetic studies performed in NHPs are desired because of the difficulty in extrapolating data on antibody biodistribution and pharmacokinetics to humans from non-primates. Such information is also necessary for immuno-PET preclinical studies [13] [14]. Animal welfare and bioresource reduction are very important issues nowadays; in this context, sharing information about the kinetics of non-target antibodies and their predicted metabolites will allow more rational use of animals for research purposes. Several studies have investigated the biodistribution and uptake of ^{89}Zr-labelled antibodies in NHPs, such as rhesus and cynomolgus monkeys. However, among these studies, only a few have specifically evaluated the distribution of ^{89}Zr-labelled human IgG using negative control antibodies as a comparator in IgG biodistribution studies. Additionally, limited research has focused on assessing the metabolites of ^{89}Zr, such as free ^{89}Zr metal and [^{89}Zr]Zr-DFO. The purpose of this study was to evaluate the in vivo distribution of ^{89}Zr-labelled anti-KLH human IgG and its metabolites in cynomolgus macaques, and to confirm their non-specific/physiological accumulation in healthy NHPs. KLH-targeting human IgG was utilised as a non-specific negative control antibody, as it does not bind specific human antigens and allows for the assessment of non-specific distribution and physiological accumulation in vivo. We consider it highly valuable to share standard data using biological resources such as NHPs, as this can enhance the robustness and reproducibility of research findings, and these standard data obtained as signals during PET imaging may be particularly useful for preclinical and NHP studies.

2. Materials and methods

2.1. [^{89}Zr]oxalate production

^{89}Zr was produced via the ^{89}Y (p,n) ^{89}Zr-nuclear reaction using a solid ^{89}Y-foil (50 × 50 × 0.1 mm) target (Fisher Scientific, Waltham, MA, USA) attached to a custom-made target. The beam was irradiated using a cyclotron (Sumitomo Heavy Industries, Tokyo, Japan). The incident proton beam energy was approximately 12 MeV, and a beam current of 25 μA was used for 50 min-target irradiations. ^{89}Zr was purified from the ^{89}Y target material using a hydroxamate resin, following the procedure described by Holland et al. [9] with some modifications, including the use of automatic refining equipment (Sumitomo Heavy Industries Ltd., Japan). The eluted [^{89}Zr]$ZrCl_4$ solution was dried and dissolved in 1 M oxalic acid to obtain highly concentrated [^{89}Zr]Zr-oxalate (50–100 MBq/20–50 μL).

2.2. Antibody conjugation with p-isothiocyanatobenzyl-desferrioxamine and radiolabelling

Anti-KLH human IgG obtained from Astellas Pharma Inc. (Tokyo, Japan) and a commercially available Fab isotype control (Southern Biotech, Birmingham, AL, USA) were used as the experimental antibodies. The coupling of the bifunctional chelate and radiolabelling was performed as described by Vosjan et al. [15]. Briefly, a 3-fold equivalent of DFO-Bz-NCS in DMSO (<2 % of the total volume) was added to the antibody dissolved in sodium bicarbonate at pH 9. The reaction mixture was incubated in a water bath at 37 °C for 1 h. Purification was performed using a size-exclusion chromatography column (PD-10, GE Healthcare, Chicago, IL, USA) and eluted with phosphate-buffered saline (PBS). The number of DFO molecules bound per antibody was determined by comparing the average molecular weights of untreated and DFO-conjugated antibodies using MALDI-TOF MS (4800 Plus MALDI TOF/TOF Analyzer, AB SCIEX, Framingham, MA). The DFO binding number was calculated as: [(average molecular weight after modification) - (average molecular weight before modification)]/(DFO molecular weight), where the average molecular weight was derived from 10 measurements per sample. The number of modified chelators introduced is 0.76–0.91 per molecule for IgG and 0.23–0.29 for Fab.

The buffer solution in which the DFO-conjugated antibodies were dissolved was exchanged with a gentisic acid solution (5 mg/mL, dissolved in 0.9 % NaCl) using a 50 k (for IgG) or 10 k (for Fab) filter. The neutralised [^{89}Zr]Zr -oxalate solution (50 μL) with 2 M sodium carbonate (22.5 μL) was mixed with 0.5 M HEPES (72.5 μL) and the antibody solution, which was dissolved in a 5 mg/mL gentisic acid/0.9 %

NaCl solution. To achieve a final concentration of 0.25 M, additional 0.5 M HEPES solution was added. The reaction mixture volume ranged from 400 to 2000 μL. The reaction mixture was incubated at room temperature for 1 h. Free ^{89}Zr metal was separated with a size exclusion chromatography column (PD-10, GE Healthcare) and eluted with gentisic acid solution to afford the [^{89}Zr]Zr -DFO-antibody. The radiochemical purity was estimated to be >95 % (based on Thin-layer chromatography (TLC) analysis). TLC was performed using a silica gel TLC plate (silica gel, 60 RP-18 F254S, Millipore) as the stationary phase and developed using 100 mM EDTA (pH 7.0) as the mobile phase. After the development, the TLC plate was analyzed using a phosphor imager (FLA-7000, Fujifilm Life Sciences) to detect the radiolabeled compounds.

2.3. Preparation of [^{89}Zr]Zr-Oxalate and [^{89}Zr]Zr-DFO Solution

[^{89}Zr]Zr-oxalate was neutralised and diluted with saline to obtain the [^{89}Zr]Zr-oxalate solution for animal injection. The [^{89}Zr]Zr-DFO solution was prepared by mixing 100 μL desferrioxamine mesylate solution (250 mg/mL) and 10 μL [^{89}Zr]Zr-oxalate solution at room temperature followed by incubation for 5 min. Then, 1 mL saline was added to obtain the [^{89}Zr]Zr-DFO solution. The [^{89}Zr]Zr-DFO was tested using TLC to confirm the absence of free ^{89}Zr metal.

2.4. Stability of ^{89}Zr-labelled IgG and Fab in macaque serum

The in vitro stability of the radiolabelled IgG and Fab in macaque serum was assessed. ^{89}Zr- labelled IgG (0.1 MBq) and ^{89}Zr-labelled Fab (0.1 MBq) were added to macaque serum, and after 24, 72, and 144 h of incubation at 37 °C for ^{89}Zr-labelled IgG, and after 60 min and 24 h for ^{89}Zr-labelled Fab, aliquots of the incubated mixtures were injected into an high-performance liquid chromatography (HPLC) equipment (column: BioSEC 3000, mobile phase: PBS pH 7.0); the eluate was fractionated, and radioactivity was quantified using a γ-counter (AccuFLEX γ7001, Hitachi Aloka Medical, Tokyo, Japan). For TLC analysis, the samples were spotted on silica gel plates (silica gel, 60 RP-18 F254S, Millipore, Billerica, MA, USA) and developed using 100 mM EDTA (pH 7.0) as the mobile phase.

2.5. ^{89}Zr- labelled IgG administration and PET

Three male cynomolgus macaque specimens weighing 2.5–3.5 kg were used for the PET measurements. The experimental procedures, including animal sacrifice, were approved by Okayama University(OKU-2014566) and the Institutional Animal Care and Use Committee of Astellas Pharma Inc.(C-T15107–01). Tsukuba Research Center is accredited by the Association for Assessment and Accreditation of Laboratory Animal Care International. Animals were housed individually in a Primate Housing System (12/12 h light dark cycle) in the Animal Resources facility of the Okayama University. The animals were given a range of environmental enrichment (e.g. toys, mirrors), provided with water ad libitum, and given a range of food options including fresh fruits. All efforts were made to provide good care and alleviate unnecessary discomfort, and no adverse events occurred. Macaques were initially anesthetised by intramuscular administration of ketamine (5 mg/kg) combined with xylazine (0.5 mg/kg). Atropine sulfate (0.05 mg/kg) was also administered intramuscularly before ketamine/xylazine injection. General anesthesia was maintained with isoflurane (1.5 %–2 %) mixed with oxygen (2 L/min) through an endotracheal tube. Vital conditions, such as pulse, oxygen saturation, end-tidal carbon dioxide pressure, and body temperature, were monitored throughout the procedure.

The following PET probes were injected intravenously via veins in the lower limb: ^{89}Zr- labelled IgG (3.9 ± 1.7 MBq/kg, n = 3), ^{89}Zr-labelled Fab (3.17 or 1.22 MBq/kg, n = 2), [^{89}Zr]Zr-DFO (0.25 MBq/kg, n = 1), [^{89}Zr]Zr-oxalate (0.24 MBq/kg, n = 1). Post-injection (p.i.) emission data were acquired using a PET/CT scanner system (Eminence STARGATE, Shimadzu, Kyoto, Japan) at different time points: 0, 1, 3, 6, and 10 days p.i. for ^{89}Zr- labelled IgG; 0–30 min p.i. for ^{89}Zr-labelled Fab; 0–150 min p.i. for [^{89}Zr]Zr-DFO, and 24 h p.i. for [^{89}Zr]Zr-oxalate. Images were reconstructed using a dynamic row-action maximum-likelihood algorithm (DRAMA). Regions of interest were drawn from axial images in fused PET/CT images. The standard uptake value (SUV) was calculated as follows: SUV = [tissue radioactivity in Bq/g tissue]/[injected radioactivity in Bq/g body weight]. To determine the clearance rate of ^{89}Zr- labelled IgG from circulation, blood samples were collected at each time point after PET scans, and ^{89}Zr- labelled IgG plasma concentrations were measured using a γ-counter (AccuFLEX γ 7001, Hitachi Aloka Medical, Tokyo, Japan). Urine was collected from the bladder using a urinary catheter after PET imaging only in ^{89}Zr-labelled Fab-injected animals.

2.6. Autoradiography, histology, and metabolite analysis in kidney and liver

After PET imaging, all macaques were euthanised by intravenous administration of sodium pentobarbital (100 mg/kg) under anesthesia. Kidneys and livers from ^{89}Zr- labelled IgG-injected macaques were removed 6 days after probe injection. The preparation of subcellular fractions was performed with modifications based on the method reported by Carina Wagner et al. [16]. Specifically, the tissues were homogenised with a Potter homogeniser in 4 volumes of ice-cold buffer (0.25 M sucrose, 10 mM HEPES, 1 mM EDTA). Nuclei and unbroken cells were sedimented by centrifugation at 1000 ×g for 10 min, and the supernatant was transferred to a clean tube. Further centrifugation of the supernatant at 15,000 ×g for 15 min led to the following subcellular fractions: the cytosolic- and microsomes-enriched fraction (Mi/Cy) in the supernatant and the mitochondria- and lysosome-enriched fraction (Mt/Ly) in the sediment. The radioactivity of each fraction was measured using a γ-counter (AccuFLEX γ 7001, Aloka), and the Mi/Cy to Mt./Ly ratio was calculated. The aqueous fraction (fraction Mi/Cy) was subjected to TLC and autoradiography (ARG) analysis. The same protocol was used to obtain subcellular fractions from the kidney lysates on the first day p.i. in macaques injected with ^{89}Zr-labelled Fab. The kidneys and livers of the macaques were excised and embedded in OCT medium (Sakura Finetek, Torrance, CA, USA). Frozen sections (7-μm thick) were used for ARG analysis (FLA-7000, Fujifilm, Tokyo, Japan). HE staining was performed according to standard procedures.

3. Results

3.1. Stability of ^{89}Zr- labelled IgG and Fab in macaque serum

Radiolabelled IgG was incubated in cynomolgus macaque serum for up to 6 days. TLC results demonstrated that >90 % of the radioactivity was retained at the origin, indicating that ^{89}Zr ions were not released from the chelators. HPLC analyses revealed that 100.0, 92.1, and 87.4 % of the original IgG radioactivity was retained at 24, 72, and 144 h, respectively, and small amounts of radioactivity were transferred to smaller molecular-sized fractions. Radiolabelled Fab was tested at 60 min and 24 h. TLC results demonstrated that >90 % of the radioactivity was retained at the origin. The stability of the ^{89}Zr-labelled Fab fraction was 98.2 % at 60 min and 75.3 % at 24 h on HPLC analyses.

3.2. Distribution of ^{89}Zr- labelled IgG

Representative whole-body PET/CT images were obtained at different times after administration of ^{89}Zr- labelled IgG to cynomolgus macaques (Fig. 1a). It may be observed that ^{89}Zr- labelled IgG is initially distributed in the blood pool (heart) and gradually migrates to the liver, kidney, and spleen. No remarkable accumulation in the bone was observed, and no excretion to the urinary bladder was observed. The time-activity curves showed that SUV decreased rapidly in the heart,

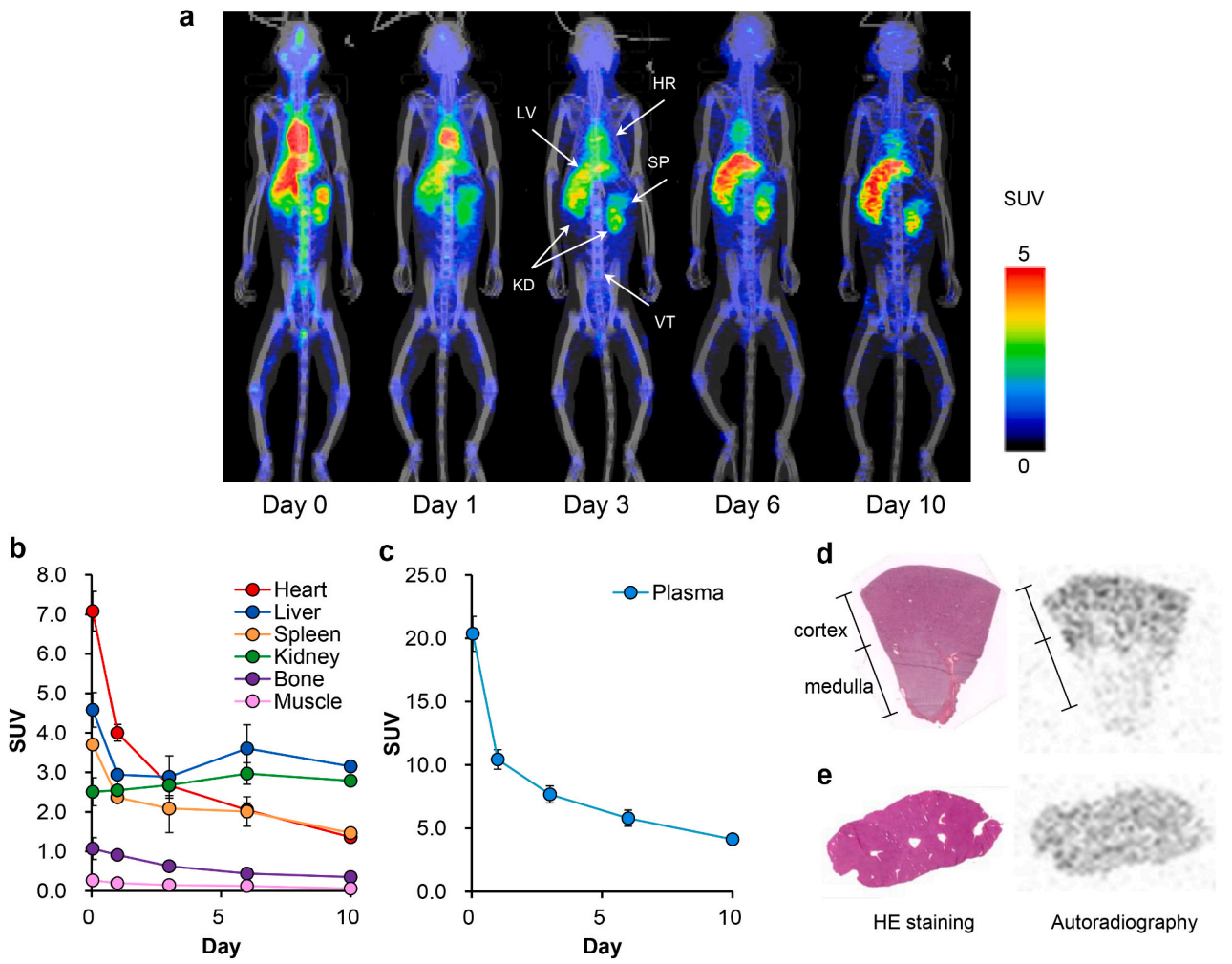

Fig. 1. Distribution of ^{89}Zr- labelled IgG in cynomolgus macaque. (**a**) Representative whole-body PET/CT images of cynomolgus macaque at 0–10 days after administration of ^{89}Zr- labelled IgG. HR, heart; LV, liver; SP, spleen; KD, kidney; VT, vertebral body (as representative bone). (**b** and **c**) Time-activity curves in individual organs and plasma, respectively. (**d** and **e**) HE staining (left) and ARG (right) of renal sections and liver, respectively.

bone, and muscle, coinciding with SUV reduction in plasma (Fig. 1b, c), whereas radioactivity increased over time in the kidneys and liver. Autoradiography of renal sections indicated that most of the radioactivity accumulated in the renal cortex (Fig. 1d), whereas the liver exhibited a more diffuse radioactivity distribution in the whole organ (Fig. 1e).

3.3. Distribution of ^{89}Zr-labelled Fab

We also evaluated the biodistribution of ^{89}Zr-Fab in these two macaques. Radioactivity in the kidneys rapidly increased and in the blood (heart) rapidly decreased after ^{89}Zr-Fab injection in both specimens (Fig. 2a-d). The cortex and renal tubules were the kidney areas with the highest radioactivity accumulation (Fig. 2e). Radioactivity was also observed in the urinary bladder of one of the specimens (Fig. 2b, d). The results of SDS-PAGE and ARG analysis performed on urine samples and unlabelled Fab revealed that Fab was excreted in the urine (Fig. 2f).

3.4. Metabolism of ^{89}Zr-antibodies

Liver lysates obtained after 6 days of ^{89}Zr-labelled IgG administration contained 42.4 % radioactivity in the mitochondria and lysosome (Mt/Ly)-enriched fraction, while the remaining 57.6 % was detected in the microsome and cytoplasm (Mi/Cy)-enriched fraction. However, almost all radioactivity was observed in the Mi/Cy-enriched fraction of renal lysates. Similarly, >90 % of radioactivity existed in the same fraction (Mi/Cy) 1 d after injection in the renal lysates obtained from animals administered ^{89}Zr-labelled Fab.

3.5. Distribution of [^{89}Zr]Zr-DFO and [^{89}Zr]Zr-oxalate

To obtain information related to ^{89}Zr metabolism in our NHP model, we selected [^{89}Zr]Zr-DFO as the minimum metabolite/fragment of the [^{89}Zr]Zr-DFO-antibody and [^{89}Zr]Zr-oxalate as the radiometal released from it. Sequential PET/CT images revealed that [^{89}Zr]Zr-DFO was mainly directed toward the urinary system, with partial accumulation in the gallbladder (Fig. 3a-c), without any evidence of bone uptake. A large amount of [^{89}Zr]Zr-DFO was excreted in the urine and gallbladder within 140 min . In contrast, [^{89}Zr]Zr-oxalate was highly accumulated in the epiphysis of the long bones and vertebral body 1 d p.i. (Fig. 3d), while the uptake was less pronounced in the bone diaphysis and medullary cavity.

4. Discussion

The general distribution patterns of ^{89}Zr- labelled IgG, ^{89}Zr-labelled Fab, [^{89}Zr]Zr-DFO, and [^{89}Zr]Zr-oxalate in cynomolgus macaques were assessed. We aimed to provide basic knowledge regarding the distribution of intact antibodies and free Zr ions, Zr-DFO or Zr-antibody fragment produced by their metabolites. The anti-KLH antibody was used as

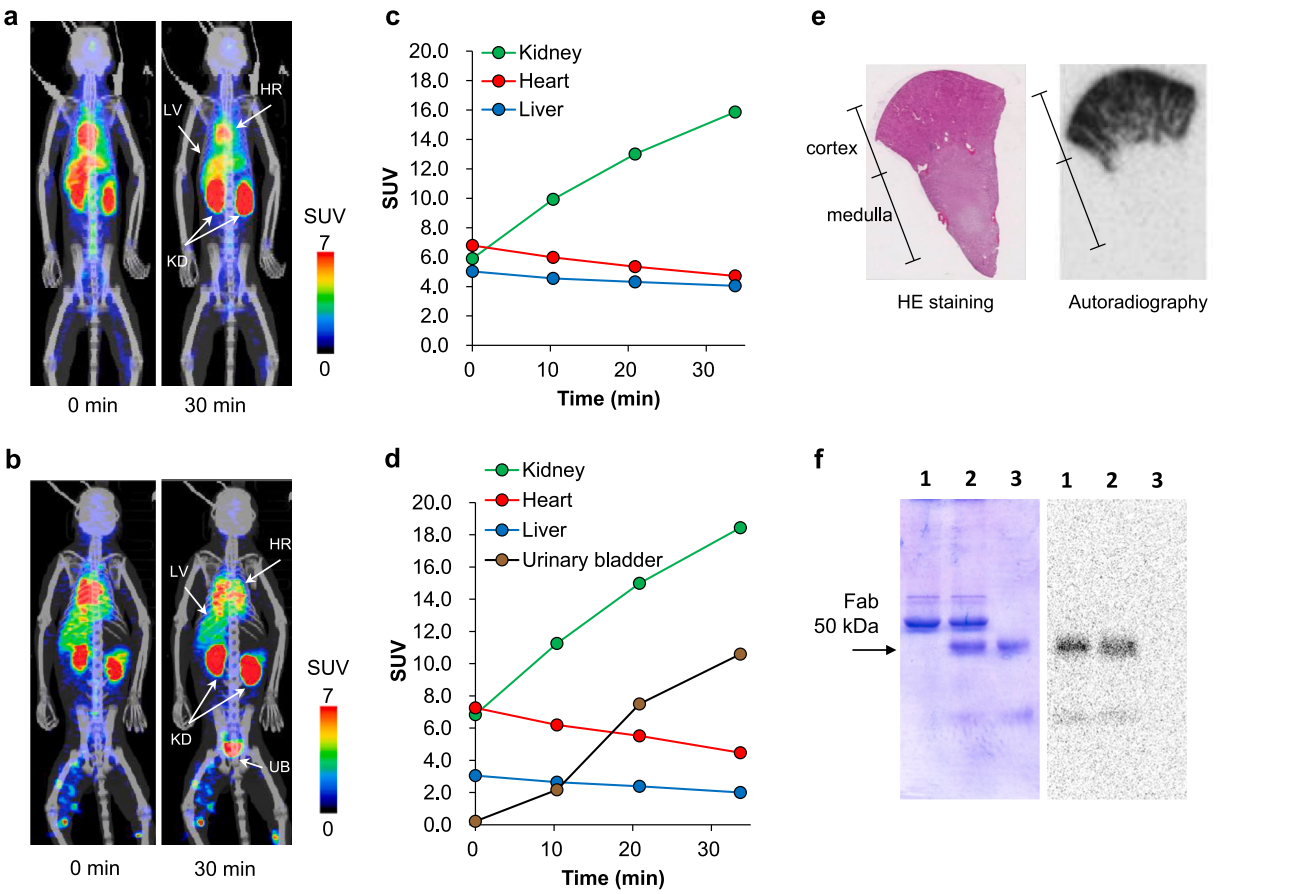

Fig. 2. Distribution of ^{89}Zr- labelled Fab in two specimens of cynomolgus macaque. (**a** and **b**) Whole-body PET/CT images at 0 (left) and 30 min (right) after administration. (**c** and **d**) Time-activity curves in individual organs. HR, heart; LV, liver; KD, kidney; UB, urinary bladder. (**e**) HE staining and ARG analysis of renal section. (**f**) SDS-PAGE (left) and ARG (right) of urine samples collected 30 min after injection. Lane 1, urine sample; lane 2, urine sample added to unlabelled Fab; lane 3, unlabelled Fab. The arrow indicates the location of the Fab subunit (50 kDa).

a negative control, showing no accumulation due to antigen-antibody interactions, thereby providing control data for the distribution of general human IgG antibodies in cynomolgus macaques. In contrast to studies employing antibodies targeting CD44 [13] or HB-EGF [14], which are unable to exclude target-specific distributions, the ^{89}Zr-labelled IgG distribution data generated with KLH antibodies in this study provide valuable reference data for comparisons with other molecule-targeting antibodies.

Immuno-PET techniques relying on ^{89}Zr-labelled IgG are advantageous for visualizing the whole-body distribution [6]. In this study, we detected ^{89}Zr-labelled IgG accumulation in the liver and kidneys of macaques at 6–10 days post-injection, based on calculated SUV and PET data. In contrast, the blood and other organs showed decreased counts at that time. When ^{89}Zr-labelled Fab, a shortened IgG variant, was administered, considerable retention of the radiolabelled compound was observed in the renal tissues (proximal tubules), and part was delivered to the urinary bladder as intact Fab. In addition, [^{89}Zr]Zr-DFO was mainly delivered to the urinary bladder and, to a lesser extent, to the gallbladder within a few hours, while [^{89}Zr]Zr-oxalate accumulated mainly in the bones.

Accumulation of radiolabelled IgG in the liver has been well documented in humans and other animals [6]; once in the liver, IgG undergoes proteolysis in the reticuloendothelial system. IgG binding to cells of the phagocytic system (macrophages and monocytes) occurs through the Fc portion of the antibody, which interacts with membrane-bound Fcγ receptors to allow subsequent endocytosis and lysosomal degradation [17]. In contrast, the fate of IgG in renal tissue is less known, and previous clinical studies have revealed variable uptake levels of ^{89}Zr-labelled therapeutic antibodies by the kidneys. Some studies conducted in humans revealed that the renal uptake of ^{89}Zr-cetuximab was only one-third of the liver uptake at 6 days p.i. [18,19]. However, variable ratios between these organs at 4–6 days p.i. were reported for other ^{89}Zr-labelled immunotherapy agents, such as ^{89}Zr-ibritumomab [20], ^{89}Zr-fresolimumab [21], and ^{89}Zr-RG7116 [22]. Only low-molecular-weight proteins, peptides, or amino acids generated during proteolysis in other organs are excreted renally [23]. We hypothesise that renal uptake may differ among IgGs because the amount and size of peptide fragments released from these molecules depend on each degradation process.

We found similar ^{89}Zr-labelled IgG blood clearance in macaques compared to humans [18,20]. The transportation and retention of intact IgG in the blood closely depend on the uptake and recycling via neonatal Fc receptor (FcRn), except for the metabolism related to the antigen-antibody response. Suzuki et al. showed that the affinity of therapeutic antibodies for FcRn correlated closely with their serum half-lives [24], and the chimeric IgG serum half-life in mice was shorter than that in humans because of the low affinity of human IgG for mouse FcRn. In contrast, human and macaque IgG have been shown to bind with similar affinities to human and cynomolgus macaque FcRn [25]. Therefore, cynomolgus macaques are more appropriate animal models than rodents for evaluating IgG blood clearance.

We found that ^{89}Zr-labelled Fab immediately accumulated in the kidneys of macaques. Generally, small antibody-derived molecules, such as Fab [26], diabody [27], and scFv [28], are filtered in the glomeruli and reabsorbed in the renal tubules. The mechanisms underlying the renal uptake of radiolabelled proteins have been previously discussed. In

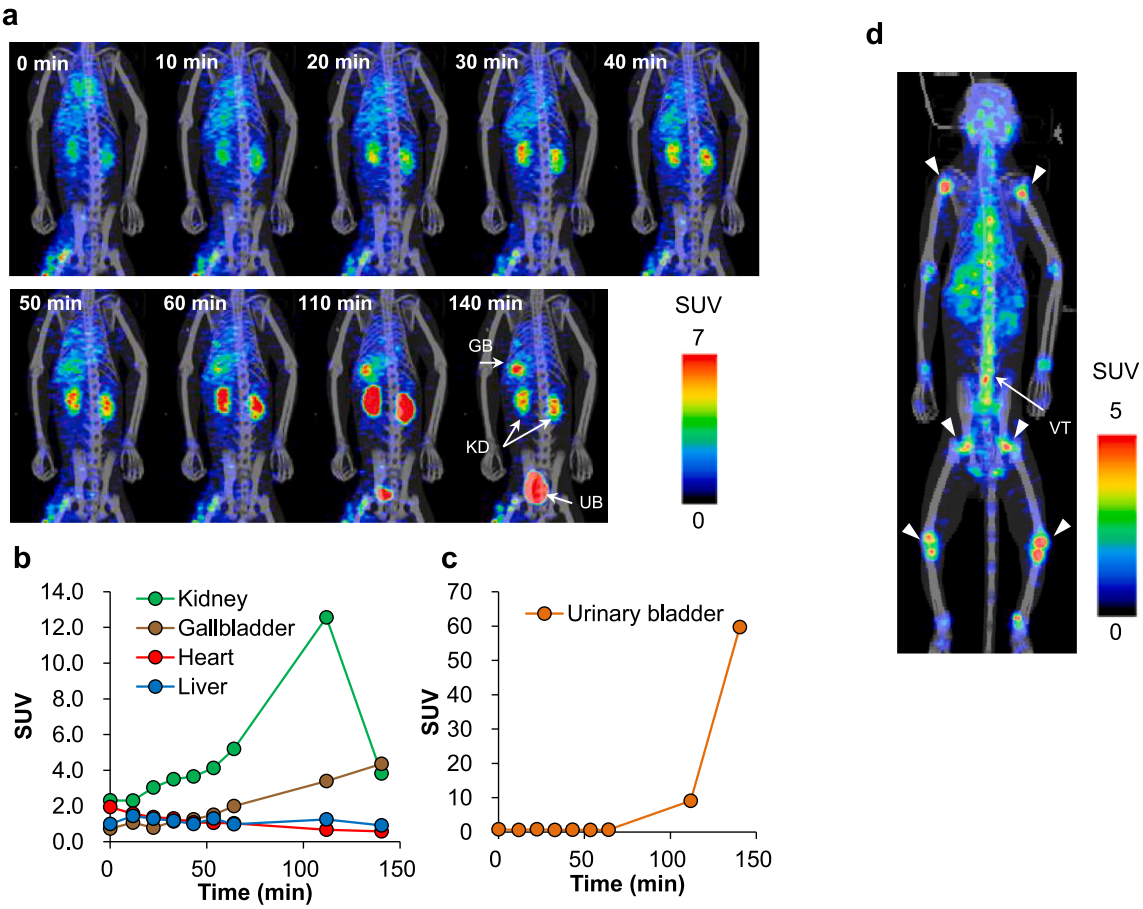

Fig. 3. Distribution of expected metabolites from ^{89}Zr- labelled IgG. (**a**) Sequential PET/CT images of a cynomolgus macaque at 0 to 140 min after administration of [^{89}Zr]DFO. (**b** and **c**) Time-activity curves in selected organs. (**d**) PET/CT image of a cynomolgus macaque at 24 h after administration of [^{89}Zr]oxalate.

this sense, megalin-cubilin receptor involvement in the renal uptake of [^{111}In]DTPA-D-Phe^1-octreotide was shown using the opossum kidney cell line [29] and kidney-specific megalin knock-out animals [30]. Because the megalin-cubilin system operates in the proximal convoluted tubules of the renal cortex, radioactivity may localise mainly in that tissue. The accumulation of ^{89}Zr-labelled Fab and IgG in the renal cortex of macaques showed a similar pattern. This finding indicates that protein/peptide fragments from IgG, including ^{89}Zr, were subjected to reuptake in the renal tubules. In line with this result, the in vitro stability test carried out using macaque serum revealed increases in radioactivity associated with the small molecular-sized fraction after 72 and 144 h of incubation.

In the urine samples from macaques that received ^{89}Zr-labelled Fab, radioactivity was excreted as ^{89}Zr- labelled Fab, revealing that appreciable amounts of intact ^{89}Zr- labelled Fab could be filtered into the urine without previous degradation. Tsai et al. [31] reported that approximately half of the radioactivity in the urine of mice after administration of ^{111}In-Rituxan-Fab corresponded to intact Fab and the remaining part to small metabolites. Conversely, peptide fragments derived from intact ^{89}Zr- labelled IgG did not seem to have been excluded from circulation into the urine; instead, the renal cells retained considerable radioactivity.

Previous reports have documented that radiolabelled proteins undergo proteolysis immediately after their internalisation into renal cells, and radioactivity may be detected in lysosomes [32]. Interestingly, we found that almost all radioactivity existed in the cytosolic fraction of the renal lysates of macaques injected with ^{89}Zr- labelled IgG; the reason for this finding remains unknown. However, because TLC analysis of the renal lysate showed that almost all radioactivity was retained at the origin part of the chromatogram, radioactivity as $^{89}Zr^{4+}$ might not exist in the renal cytosol.

The liver and kidney lysates of macaques exhibited different lysosome–cytosol radioactivity ratios. Radioactivity in the lysosome fraction obtained from the liver might represent undigested ^{89}Zr- labelled IgG protein, while antibodies internalised into renal cells are expected to be immediately degraded in lysosomes, from which small radiolabelled fragments might go out and reach the cytosol. Rogers et al. indicated that ^{111}In-F(ab)'2 was degraded into [^{111}In]lys at 1 d post-injection in rat kidney lysates, although larger radiolabelled molecules remained in the liver lysates [33].

PET imaging studies performed in macaques injected with [^{89}Zr]Zr-oxalate showed important activity in the bones, especially in the epiphysis of the long bones and vertebral body. [^{89}Zr]Zr-oxalate is thought to be equivalent to $^{89}Zr^{4+}$. In mice, [^{89}Zr]Zr-oxalate, [^{89}Zr]Zr-citrate, and [^{89}Zr]Zr-chloride had a strong affinity for bones and joints [12,34]. It is very likely that ^{89}Zr is chelated by hydroxyapatite, a phosphate constituent of bones and epiphysis; the extracted marrow cells were insignificantly radioactive compared to the calcified tissues (0.1 % of the total activity of the bones). Since $^{89}Zr^{4+}$ may be released from the [^{89}Zr]Zr-DFO-antibody, the radioactivity in the bone might increase with time. In this study, $^{89}Zr^{4+}$ was scarcely released from DFO-IgG and did not return to circulation, which could be attributed to the decreased bone uptake over time observed in macaques administered with ^{89}Zr- labelled IgG and TLC data in the stability test. Additionally, [^{89}Zr]Zr-DFO was rapidly excreted into the urine and gallbladder. Therefore, after [^{89}Zr]Zr-DFO-antibody administration, it is reasonable to expect that specific cleavage of intact [^{89}Zr]Zr-DFO from the antibody would not lead to ^{89}Zr bone uptake, as it would immediately be excreted.

In a similar vein, the pharmacokinetics of [^{89}Zr]Zr-oxalate observed in mice were found to be consistent with those in NHPs, and the pharmacokinetics of [^{89}Zr]Zr-DFO also appeared to be similar between mice and NHPs [34]. Berg et al. [7] conducted a study on the pharmacokinetics of ^{89}Zr-labelled antibodies targeting herpesvirus glycoprotein D (gD) in NHP over 30 days, comparing the performance of four chelators. Their findings of activity in the bladder and gastrointestinal tract are consistent with the results of our study on [^{89}Zr]Zr-DFO and ^{89}Zr-labelled Fab distribution. Furthermore, our data demonstrated that the distribution of metabolites and impurities in ^{89}Zr- labelled IgG could be clearly identified, thereby highlighting the utility of the data obtained in this research.

The initial metabolites of radiolabelled antibodies, such as ^{89}Zr-labelled IgG, are typically derived from chelating agents, particularly $^{89}Zr^{4+}$ or [^{89}Zr]Zr-DFO [12]. In light of the established metabolic pathways of antibodies, it seems highly plausible that these molecules undergo internalisation through Fc receptor-mediated phagocytosis, followed by lysosomal degradation and subsequent excretion [35]. However, in this study, not all of the proposed metabolites could be identified or replicated. As a case study, we investigated the distribution of these metabolites in the body using ^{89}Zr-labelled Fab, a smaller antibody fragment containing [^{89}Zr]Zr-DFO. This limitation highlights the need for further research to fully elucidate the metabolic pathways and distribution of radiolabel antibody fragments in vivo. Additionally, this study is limited by the provision of only short-term distribution data for ^{89}Zr- labelled IgG byproducts, and moreover, the absence of long-term distribution data for these metabolites represents a significant limitation. The initial metabolites of radiolabelled antibodies, such as ^{89}Zr-labelled IgG, are primarily derived from chelating agents, particularly $^{89}Zr^{4+}$ or [^{89}Zr]Zr-DFO [12]. Based on established metabolic pathways, it is highly plausible that these molecules undergo internalisation via Fc receptor-mediated phagocytosis, followed by lysosomal degradation and subsequent excretion [35]. However, in this study, not all putative metabolites could be identified or characterized. As a case study, we investigated the biodistribution of these metabolites using ^{89}Zr-labelled Fab, a smaller antibody fragment containing [^{89}Zr]Zr-DFO. This limitation highlights the need for further investigations to fully elucidate the metabolic pathways and biodistribution of radiolabelled antibody fragments in vivo. Furthermore, this study is limited by the provision of only short-term distribution data for ^{89}Zr-labelled IgG byproducts, and the absence of long-term distribution data for these metabolites remains a significant limitation. Additionally, this study did not include a detailed assessment of bone uptake, despite the availability of ex vivo data. PET imaging revealed notable ^{89}Zr uptake in the joints, including the knees, elbows, wrists, and ankles; however, it remains unclear whether this accumulation occurred in the bone itself or in the synovial fluid. Unlike the detailed renal analysis performed in this study, no joints were excised for molecular characterization or precise localization of ^{89}Zr retention. Given that [^{89}Zr]Zr-oxalate demonstrated pronounced uptake in the joints, future studies should incorporate histological analysis and molecular species identification to distinguish between bone and synovial accumulation. Another limitation of this study is the absence of direct measurement of the isoelectric point (pI) of the radiolabelled IgG. Instead, our discussion was based on theoretical estimations. Specifically, when a single DFO molecule binds to an amino group of the antibody, the +1 charge of the amino group is neutralised (±0) due to conjugation with DFO. Since the net charge of the DFO-Zr complex has been reported to be +1, the overall net charge of the modified antibody is estimated to be approximately equivalent to that of the unmodified antibody. This estimation is supported by previously reported net charge values of the DFO-Zr complex [36]. A more comprehensive analysis incorporating direct pI measurements would further enhance the understanding of the physicochemical properties and in vivo behavior of radiolabelled antibodies.

5. Conclusion

In this study, we assessed the physiological distribution of anti-KLH human IgG in cynomolgus macaques using sequential PET imaging for up to 10 days. Our results demonstrate that both intact ^{89}Zr- labelled IgG and its metabolites physiologically accumulate in the kidneys and liver. Considering that ^{89}Zr- labelled Fab accumulated predominantly in the kidneys, it is expected that small fragments containing ^{89}Zr derived from this radiolabelled IgG would accumulate in renal portions or be excluded through the urine. In addition, images obtained from macaques injected with [^{89}Zr]Zr-oxalate and [^{89}Zr]Zr-DFO revealed bone accumulation and immediate exclusion, respectively. Because images obtained after ^{89}Zr- labelled IgG injection did not show remarkable accumulation in the epiphysis of long bones, we hypothesise that ^{89}Zr metal was not released from the chelator.

CRediT authorship contribution statement

Takanori Sasaki: Writing – review & editing, Writing – original draft, Visualization, Validation, Supervision, Project administration, Methodology, Data curation. **Sadaaki Kimura:** Writing – review & editing, Writing – original draft, Resources, Project administration, Methodology, Investigation, Formal analysis, Data curation. **Akihiro Noda:** Writing – review & editing, Writing – original draft, Software, Resources, Methodology, Data curation. **Yoshihiro Murakami:** Writing – review & editing, Writing – original draft, Resources, Formal analysis, Data curation. **Sosuke Miyoshi:** Writing – review & editing, Writing – original draft, Resources, Funding acquisition, Conceptualization. **Masaru Akehi:** Writing – review & editing, Writing – original draft, Data curation. **Kazuhiko Ochiai:** Writing – review & editing. **Masami Watanabe:** Writing – review & editing, Validation. **Takahiro Higuchi:** Writing – review & editing. **Eiji Matsuura:** Funding acquisition.

Ethics approval

All animal experimental procedures were approved by Okayama University(OKU-2014566) and the Institutional Animal Care and Use Committee of Astellas Pharma Inc.(C-T15107–01). Tsukuba Research Center is accredited by the Association for Assessment and Accreditation of Laboratory Animal Care International.

Funding

This work was supported by Astellas Pharma Inc. and JSPS Fostering Joint International Research (B), Grant Number 19KK0215.

Declaration of competing interest

The authors declare that they have no known competing financial interests or personal relationships that could have appeared to influence the work reported in this paper.

Acknowledgments

The experiments were performed by using the Okayama Medical Innovation Center facility at Okayama University and we acknowledged Hiroyuki Hirano (SHI Accelerator Service Ltd., Tokyo, Japan) for operating Cyclotron. We thank Department of Animal Resources, Advanced Science Research Center, Okayama University; and Radiation Research Shikata Laboratory, Advanced Science Research Center, Okayama University, for using shared equipment and animal care.

Data availability

The datasets generated during and/or analyzed during the current study are available from the corresponding author on reasonable

request. The datasets and materials held by Astellas Pharma Inc. are not publicly available due to proprietary restrictions.

References

[1] Tabrizi MA, Roskos LK. Preclinical and clinical safety of monoclonal antibodies. Drug Discov Today 2007;12(13–14):540–7. https://doi.org/10.1016/j.drudis.2007.05.010 [PubMed PMID: 17631248].

[2] Chapman KL, Pullen N, Andrews L, Ragan I. The future of non-human primate use in mAb development. Drug Discov Today 2010;15(5–6):235–42. Epub 2010/01/26, https://doi.org/10.1016/j.drudis.2010.01.002. 20096369.

[3] Lee HJ, Ehlerding EB, Cai W. Antibody-based tracers for PET/SPECT imaging of chronic inflammatory diseases. Chembiochem 2019;20(4):422–36. https://doi.org/10.1002/cbic.201800429. PubMed PMID: 30240550; PubMed Central PMCID: PMCPMC6377337.

[4] Henry KE, Ulaner GA, Lewis JS. Human epidermal growth factor receptor 2-targeted PET/single- photon emission computed tomography imaging of breast Cancer: noninvasive measurement of a biomarker integral to tumor treatment and prognosis. PET Clin 2017;12(3):269–88. https://doi.org/10.1016/j.cpet.2017.02.001. PubMed PMID: 28576166; PubMed Central PMCID: PMCPMC5545121.

[5] Colombo I, Overchuk M, Chen J, Reilly RM, Zheng G, Lheureux S. Molecular imaging in drug development: Update and challenges for radiolabeled antibodies and nanotechnology. Methods (San Diego, Calif). 2017;130:23–35. Epub 2017/07/27. doi:https://doi.org/10.1016/j.ymeth.2017.07.018. PubMed PMID: 28743635.

[6] van Dongen GAMS, Visser GWM, Hooge MNL-d, De Vries EG, Perk LR. Immuno-PET: a navigator in monoclonal antibody development and applications. Oncologist. 2007;12(12):1379–89. doi:https://doi.org/10.1634/theoncologist.12-12-1379. PubMed PMID: WOS:000252087700001.

[7] Berg E, Gill H, Marik J, Ogasawara A, Williams S, van Dongen G, et al. Total-body PET and highly stable chelators together enable meaningful ⁸⁹Zr-antibody PET studies up to 30 days after injection. J Nucl Med 2020;61(3):453–60. https://doi.org/10.2967/jnumed.119.230961. PubMed PMID: WOS:000518436700030.

[8] Perk LR, Vosjan MJ, Visser GW, Budde M, Jurek P, Kiefer GE, et al. p-Isothiocyanatobenzyl-desferrioxamine: a new bifunctional chelate for facile radiolabeling of monoclonal antibodies with zirconium-89 for immuno-PET imaging. Eur J Nucl Med Mol Imaging. 2010;37(2):250–9. Epub 2009/09/19. doi:https://doi.org/10.1007/s00259-009-1263-1. PubMed PMID: 19763566; PubMed Central PMCID: PMCPMC2816257.

[9] Holland JP, Sheh Y, Lewis JS. Standardized methods for the production of high specific-activity zirconium-89. Nuclear medicine and biology. 2009;36(7):729–39. Epub 2009/09/02. doi:https://doi.org/10.1016/j.nucmedbio.2009.05.007. PubMed PMID: 19720285; PubMed Central PMCID: PMCPMC2827875.

[10] McKnight BN, Viola-Villegas NT. ^{89}Zr-ImmunoPET companion diagnostics and their impact in clinical drug development. J Labelled Comp Radiopharm 2018;61(9):727–38. https://doi.org/10.1002/jlcr.3605. PubMed PMID: 29341222; PubMed Central PMCID: PMCPMC6050145.

[11] Holland JP, Divilov V, Bander NH, Smith-Jones PM, Larson SM, Lewis JS. ^{89}Zr-DFO-J591 for immunoPET of prostate-specific membrane antigen expression in vivo. Journal of nuclear medicine : official publication, Society of Nuclear Medicine. 2010;51(8):1293–300. Epub 2010/07/28. doi:https://doi.org/10.2967/jnumed.110.076174. PubMed PMID: 20660376; PubMed Central PMCID: PMCPMC2998794.

[12] Abou DS, Ku T, Smith-Jones PM. In vivo biodistribution and accumulation of ^{89}Zr in mice. Nuclear medicine and biology. 2011;38(5):675–81. Epub 2011/07/02. doi:https://doi.org/10.1016/j.nucmedbio.2010.12.011. PubMed PMID: 21718943; PubMed Central PMCID: PMCPMC4527328.

[13] Vugts DJ, Heuveling DA, Stigter-van Walsum M, Weigand S, Bergstrom M, van Dongen GA, et al. Preclinical evaluation of ^{89}Zr-labeled anti-CD44 monoclonal antibody RG7356 in mice and cynomolgus monkeys: Prelude to Phase 1 clinical studies. MAbs. 2014;6(2):567–75. Epub 2014/02/05. doi:https://doi.org/10.4161/mabs.27415. PubMed PMID: 24492295; PubMed Central PMCID: PMCPMC3984344.

[14] Kasai N, Adachi M, Yamano K. Preclinical pharmacokinetics evaluation of anti-heparin-binding EGF-like growth factor (HB-EGF) monoclonal antibody using Cynomolgus monkeys via ^{89}Zr-immuno-PET study and the determination of drug concentrations in serum and cerebrospinal fluid. Pharm Res 2016;33(2):476–86. Epub 2015/10/16, https://doi.org/10.1007/s11095-015-1803-2. 26464296.

[15] Vosjan MJ, Perk LR, Visser GW, Budde M, Jurek P, Kiefer GE, et al. Conjugation and radiolabeling of monoclonal antibodies with zirconium-89 for PET imaging using the bifunctional chelate p-isothiocyanatobenzyl-desferrioxamine. Nat Protoc 2010;5(4):739–43. https://doi.org/10.1038/nprot.2010.13 [PubMed PMID: 20360768].

[16] Wagner C, Hois V, Eggeling A, Pusch L, Pajed L, Starlinger P, et al. KIAA1363 affects retinyl ester turnover in cultured murine and human hepatic stellate cells. J Lipid Res 2022;63. doi:https://doi.org/10.1016/j.jlr.2022.100173. PubMed PMID: WOS:000767366300003.

[17] Wohlrab J. Pharmacokinetic characteristics of therapeutic antibodies. J Dtsch Dermatol Ges 2015;13(6):530–4. Epub 2015/05/29, https://doi.org/10.1111/ddg.12648. 26018364.

[18] Makris NE, Boellaard R, van Lingen A, Lammertsma AA, van Dongen GA, Verheul HM, et al. PET/CT-derived whole-body and bone marrow dosimetry of ^{89}Zr-cetuximab. Journal of nuclear medicine : official publication, Society of Nuclear Medicine 2015;56(2):249–54. Epub 2015/01/24, https://doi.org/10.2967/jnumed.114.147819. 25613538.

[19] Menke-van der Houven van Oordt CW, Gootjes EC, Huisman MC, Vugts DJ, Roth C, Luik AM, et al. ^{89}Zr-cetuximab PET imaging in patients with advanced colorectal cancer. Oncotarget. 2015;6(30):30384–93. Epub 2015/08/27. doi:10.18632/oncotarget.4672. PubMed PMID: 26309164; PubMed Central PMCID: PMCPMC4745807.

[20] Rizvi SN, Visser OJ, Vosjan MJ, van Lingen A, Hoekstra OS, Zijlstra JM, et al. Biodistribution, radiation dosimetry and scouting of ^{90}Y-ibritumomab tiuxetan therapy in patients with relapsed B-cell non-Hodgkin's lymphoma using ^{89}Zr-ibritumomab tiuxetan and PET. Eur J Nucl Med Mol Imaging. 2012;39(3):512–20. Epub 2012/01/06. doi:https://doi.org/10.1007/s00259-011-2008-5. PubMed PMID: 22218876; PubMed Central PMCID: PMCPMC3276758.

[21] den Hollander MW, Bensch F, Glaudemans AW, Oude Munnink TH, Enting RH, den Dunnen WF, et al. TGF-beta antibody uptake in recurrent high-grade glioma imaged with ^{89}Zr-Fresolimumab PET. Journal of nuclear medicine : official publication, Society of Nuclear Medicine 2015;56(9):1310–4. Epub 2015/07/03, https://doi.org/10.2967/jnumed.115.154401. 26135113.

[22] Terwisscha van Scheltinga AG, Lub-de Hooge MN, Abiraj K, Schroder CP, Pot L, Bossenmaier B, et al. ImmunoPET and biodistribution with human epidermal growth factor receptor 3 targeting antibody ^{89}Zr-RG7116. mAbs. 2014;6(4):1051–8. Epub 2014/05/30. doi:https://doi.org/10.4161/mabs.29097. PubMed PMID: 24870719; PubMed Central PMCID: PMCPMC4171008.

[23] Maack T, Johnson V, Kau ST, Figueiredo J, Sigulem D. Renal filtration, transport, and metabolism of low-molecular-weight proteins: a review. Kidney Int 1979;16(3):251–70. Epub 1979/09/01. PubMed PMID: 393891.

[24] Suzuki T, Ishii-Watabe A, Tada M, Kobayashi T, Kanayasu-Toyoda T, Kawanishi T, et al. Importance of neonatal FcR in regulating the serum half-life of therapeutic proteins containing the Fc domain of human IgG1: a comparative study of the affinity of monoclonal antibodies and Fc-fusion proteins to human neonatal FcR. Journal of immunology (Baltimore, Md : 1950). 2010;184(4):1968–76. Epub 2010/01/20. doi:https://doi.org/10.4049/jimmunol.0903296. PubMed PMID: 20083659.

[25] Dall'Acqua WF, Kiener PA, Wu H. Properties of human IgG1s engineered for enhanced binding to the neonatal fc receptor (FcRn). J Biol Chem 2006;281(33):23514–24. Epub 2006/06/24, https://doi.org/10.1074/jbc.M604292200. 16793771.

[26] Mendler CT, Gehring T, Wester HJ, Schwaiger M, Skerra A. ^{89}Zr-labeled versus ^{124}I-labeled alphaHER2 fab with optimized plasma half-life for high-contrast tumor imaging in vivo. Journal of nuclear medicine : official publication, Society of Nuclear Medicine 2015;56(7):1112–8. Epub 2015/05/23, https://doi.org/10.2967/jnumed.114.149690. 25999431.

[27] Viola-Villegas NT, Sevak KK, Carlin SD, Doran MG, Evans HW, Bartlett DW, et al. Noninvasive Imaging of PSMA in prostate tumors with ^{89}Zr-Labeled huJ591 engineered antibody fragments: the faster alternatives. Molecular pharmaceutics. 2014;11(11):3965–73. Epub 2014/05/02. doi:https://doi.org/10.1021/mp500164r. PubMed PMID: 24779727; PubMed Central PMCID: PMCPMC4224519.

[28] Sasaki T, Kobayashi K, Kita S, Kojima K, Hirano H, Shen L, et al. In vivo distribution of single chain variable fragment (scFv) against atherothrombotic oxidized LDL/beta2-glycoprotein I complexes into atherosclerotic plaques of WHHL rabbits: implication for clinical PET imaging. Autoimmun Rev 2017;16(2):159–67. Epub 2016/12/19, https://doi.org/10.1016/j.autrev.2016.12.007. 27988435.

[29] Barone R, Van Der Smissen P, Devuyst O, Beaujean V, Pauwels S, Courtoy PJ, et al. Endocytosis of the somatostatin analogue, octreotide, by the proximal tubule-derived opossum kidney (OK) cell line. Kidney Int 2005;67(3):969–76. Epub 2005/02/09, https://doi.org/10.1111/j.1523-1755.2005.00160.x. 15698435.

[30] de Jong M, Barone R, Krenning E, Bernard B, Melis M, Visser T, et al. Megalin is essential for renal proximal tubule reabsorption of ^{111}In-DTPA-octreotide. Journal of nuclear medicine : official publication, Society of Nuclear Medicine 2005;46(10):1696–700. Epub 2005/10/06. PubMed PMID: 16204720.

[31] Tsai SW, Li L, Williams LE, Anderson AL, Raubitschek AA, Shively JE. Metabolism and renal clearance of ^{111}In-labeled DOTA-conjugated antibody fragments. Bioconjug Chem 2001;12(2):264–70. Epub 2001/04/21. PubMed PMID: 11312688.

[32] Duncan JR, Welch MJ. Intracellular metabolism of indium-111-DTPA-labeled receptor targeted proteins. Journal of nuclear medicine : official publication, Society of Nuclear Medicine 1993;34(10):1728–38. Epub 1993/10/01. PubMed PMID: 8410290.

[33] Rogers BE, Franano FN, Duncan JR, Edwards WB, Anderson CJ, Connett JM, et al. Identification of metabolites of ^{111}In-diethylenetriaminepentaacetic acid-monoclonal antibodies and antibody fragments in vivo. Cancer Res 1995;55 (23 Suppl):5714s–20s. Epub 1995/12/01. PubMed PMID: 7493333.

[34] Deri M, Zeglis B, Francesconi L, Lewis J. PET imaging with ^{89}Zr: from radiochemistry to the clinic. Nucl Med Biol 2013;40(1):3–14. https://doi.org/10.1016/j.nucmedbio.2012.08.004. PubMed PMID: WOS:000312420000002.

[35] Ryman JT, Meibohm B. Pharmacokinetics of monoclonal antibodies. CPT Pharmacometrics Syst Pharmacol 2017;6(9):576–88 [PubMed PMID: 28653357].

[36] Cho H, Al-Saden N, Lam H, Möbus J, Reilly R, Winnik M. A comparison of DFO and DFO* conjugated to trastuzumab-DM1 for complexing 89Zr - in vitro stability and in vivo microPET/CT imaging studies in NOD/SCID mice with HER2-positive SK-OV-3 human ovarian cancer xenografts. Nucl Med Biol 2020;84-85:11–9. https://doi.org/10.1016/j.nucmedbio.2019.12.009. PubMed PMID: WOS:000536123000002.